Electronic Supplementary Material (ESI) for Journal of Materials Chemistry A.
This journal is © The Royal Society of Chemistry 2018

Supplementary Information

Air-Processed Mixed-Cation $Cs_{0.15}FA_{0.85}PbI_3$ Planar Perovskite Solar Cells Derived from PbI_2-CsI-FAI Intermediate Complex

Xiuwen Xu,[ab] Chunqing Ma,[c] Yue-Min Xie,[ab] Yuanhang Cheng,[ab] Yameng Tian,[ab] Menglin Li,[ab] Yuhui Ma,[ab] Chun-Sing Lee,[c] and Sai-Wing Tsang [ab]*

a Department of Materials Science and Engineering, City University of Hong Kong, Hong Kong SAR, P. R. China

b City University of Hong Kong Shenzhen Research Institute, Shenzhen, 518057, P. R. China

c Center of Super-Diamond and Advanced Films (COSDAF) and Department of Chemistry, City University of Hong Kong, Hong Kong SAR, P. R. China

Corresponding E-mail: saitsang@cityu.edu.hk

Table S1 Summary of solution processed perovskite solar cells prepared in ambient air with different humidity

Perovskite	Method	RH, %	PCE, %	Ref
$MAPbI_3$	Two-step (MAI dripping)	-	13.07	1
	One-Step	-	13.29	2
	One-Step	-	3.3	3
	Preheating assisted two-step	-	10.51	4
	One-step	28	16.15	5
	Two-step	35±5	10.65	6
	One-step (MAK)	40±5	17.71	7
	Two-step	40	12.73	8
	One-step	45	14.08	9
	Gas assisted two-step	42-48	16.32	10
	NH_4Cl modified one-step	45	15.60	11
	Doctor blading	45	11.29	12
	Preheating assisted two-step	50	15.76	13
	IPA modified two-step	50	15.10	14
	Two-step	50	6.80	15
	One-step (excessive MAI)	50	18.26	16
	Spray deposition	50	7.89	17
	One-step	50±5	9.2	18
	Additive modified one-step	55±5	18.20	19
	One-step	60	11.10	20
	Preheating assisted two-step	70	18.11	21
	Two-step	75	7.19	22
	Ethyl acetate assisted one-step	75	15.00	23
$MAPbI_{3-x}Cl_x$	One-step	40	16.70	24
	One-step	50	5.67	25
	Two-step	60	17.56	26
$MAPb(SCN)_xI_{3-x}$	Two-step	70	15.12	27
$CsPb_{0.9}Sn_{0.1}IBr_2$	Two-step	50-60	11.30	28
$CsPbBr_3$	Two-step	50-60	6.70	29
$Cs_{0.15}FA_{0.85}PbI_3$	Intermediate films and preheating assisted two-step	70	15.56	Our work

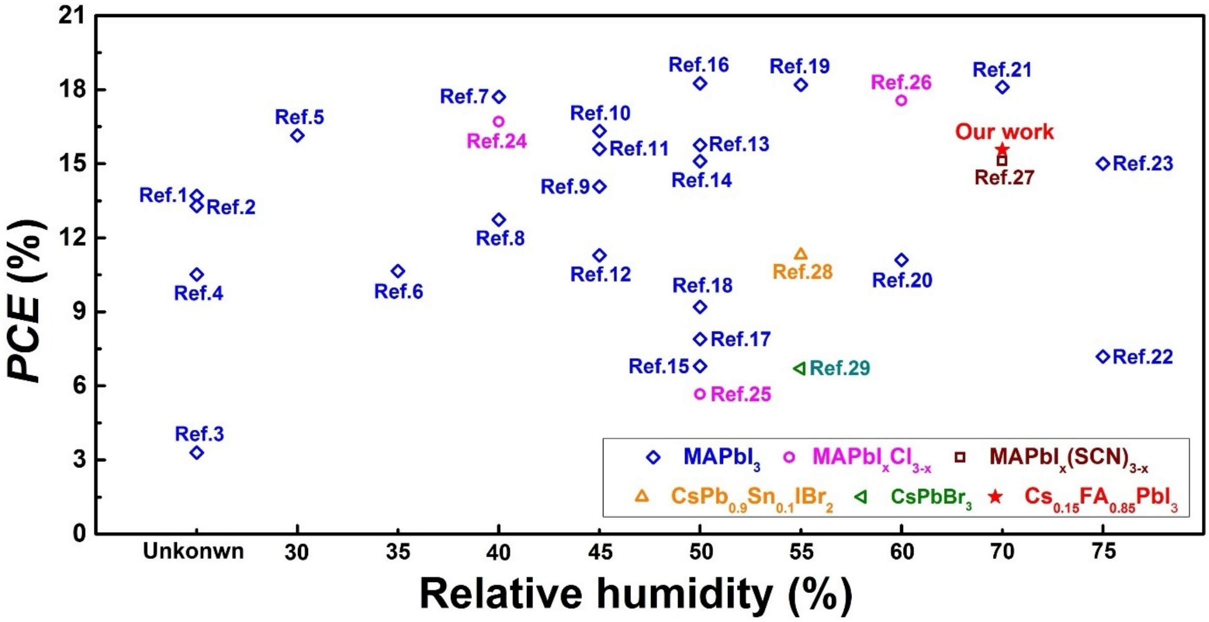

Figure S1. Summary of solution processed PSCs prepared in ambient air reported to date.

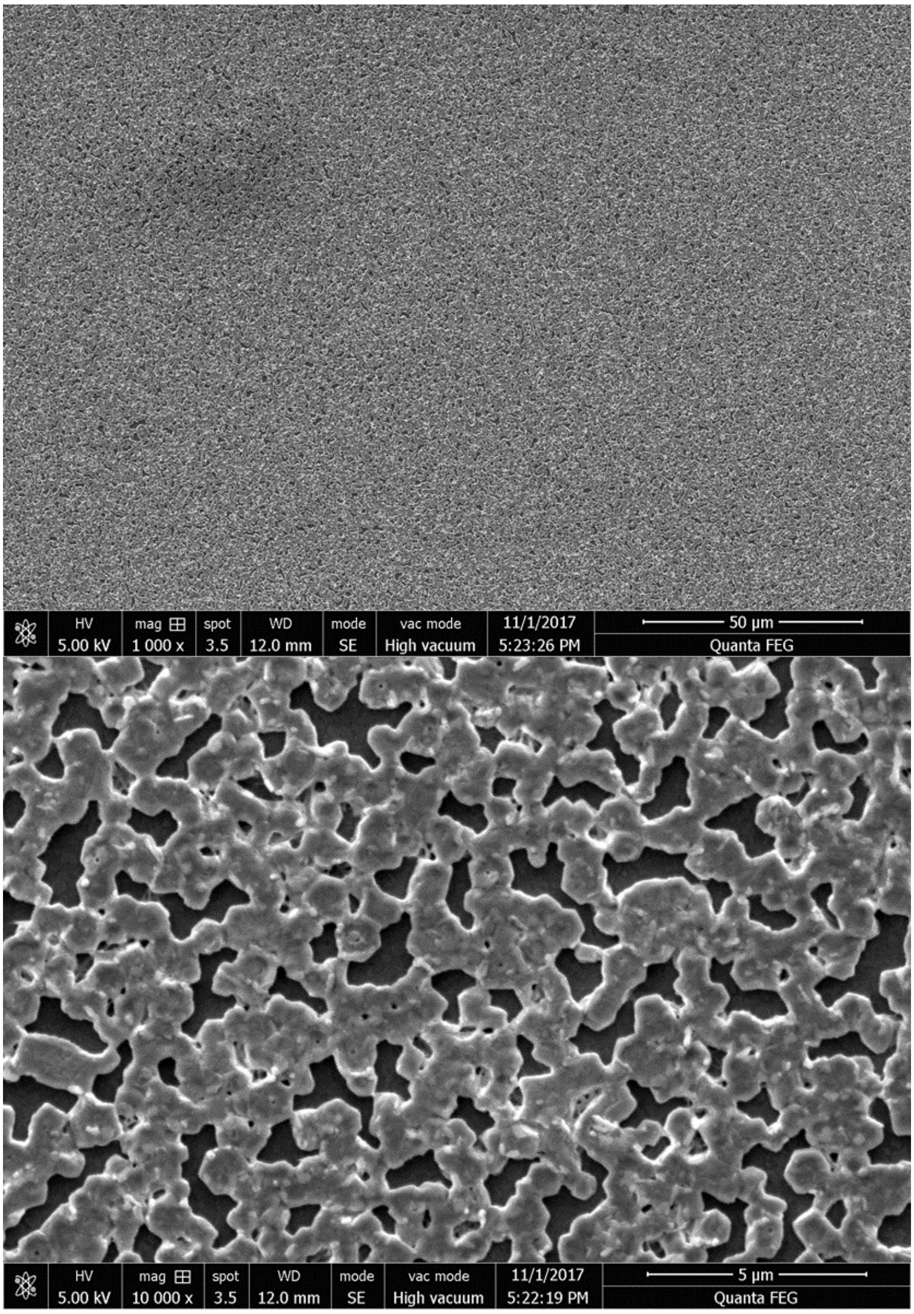

Figure S2. SEM images of the $Cs_{0.15}FA_{0.85}PbI_3$ film prepared by a preheating-assisted one-step spin coating method (x=0.85) in ambient air (RH:70±10%).

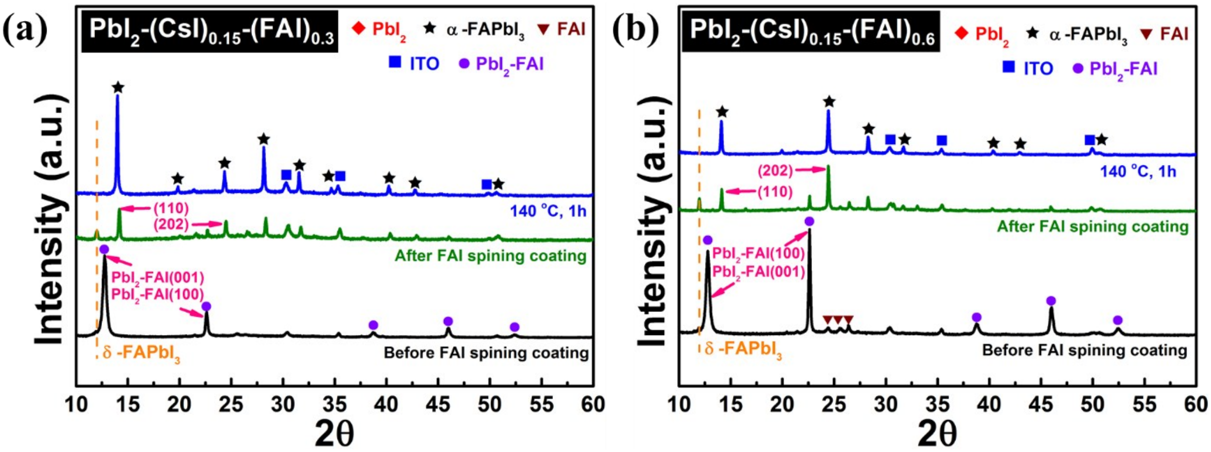

Figure S3. The evolution of XRD patterns of $Cs_{0.15}FA_{0.85}PbI_3$ derived from the PbI_2-$(CsI)_{0.15}$-$(FAI)_x$ intermediate complex films: (a) x=0.3; (b) x=0.6.

To understand the origin of perovskite orientation changes, the evolution of XRD patterns of perovskites derived from PbI_2-$(CsI)_{0.15}$-$(FAI)_{0.3}$ and PbI_2-$(CsI)_{0.15}$-$(FAI)_{0.6}$ are compared, as illustrated in **Figure S3**. Obviously, the relative intensity of (001)/(100) peaks of PbI_2-FAI in the intermediate films determines that of (110)/(202) peaks in the perovskite films. Since (202) peaks are observed in all the cases (x=0-0.85), which means the perovskite growth along (202) facet is thermodynamically feasible. Therefore, the different relative intensity of (110)/(202) peaks is caused by the different growth kinetics of (110) and (202) facets. Due to the complicated growth process, we can only conclude that the formation of (100) facets of PbI_2-FAI might be favorable for the perovskite growth along (202) facet.

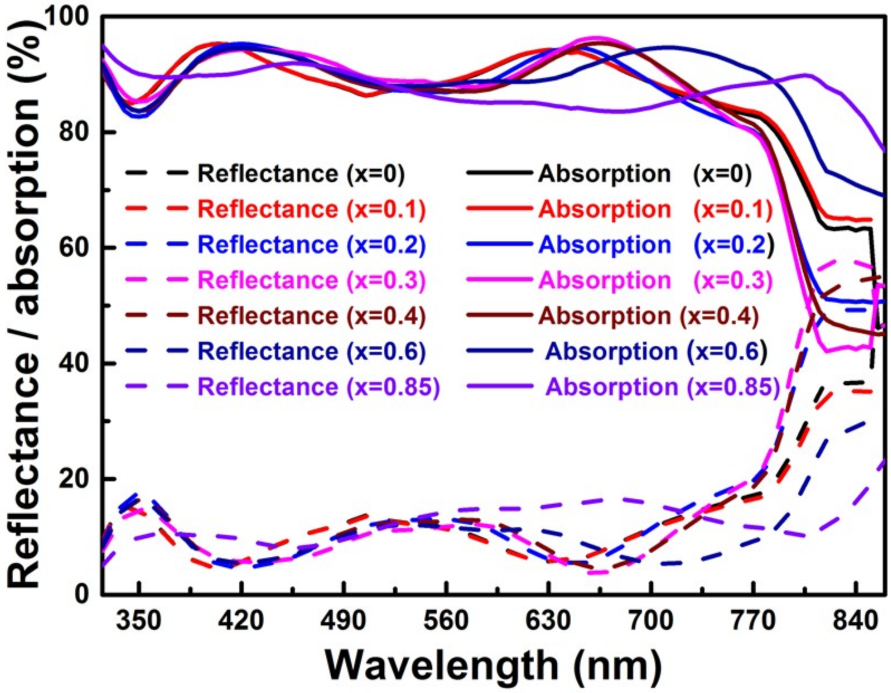

Figure S4. Reflectance and absorption of the devices based on $Cs_{0.15}FA_{0.85}PbI_3$ derived the PbI_2-$(CsI)_{0.15}$-$(FAI)_x$ intermediate complex films.

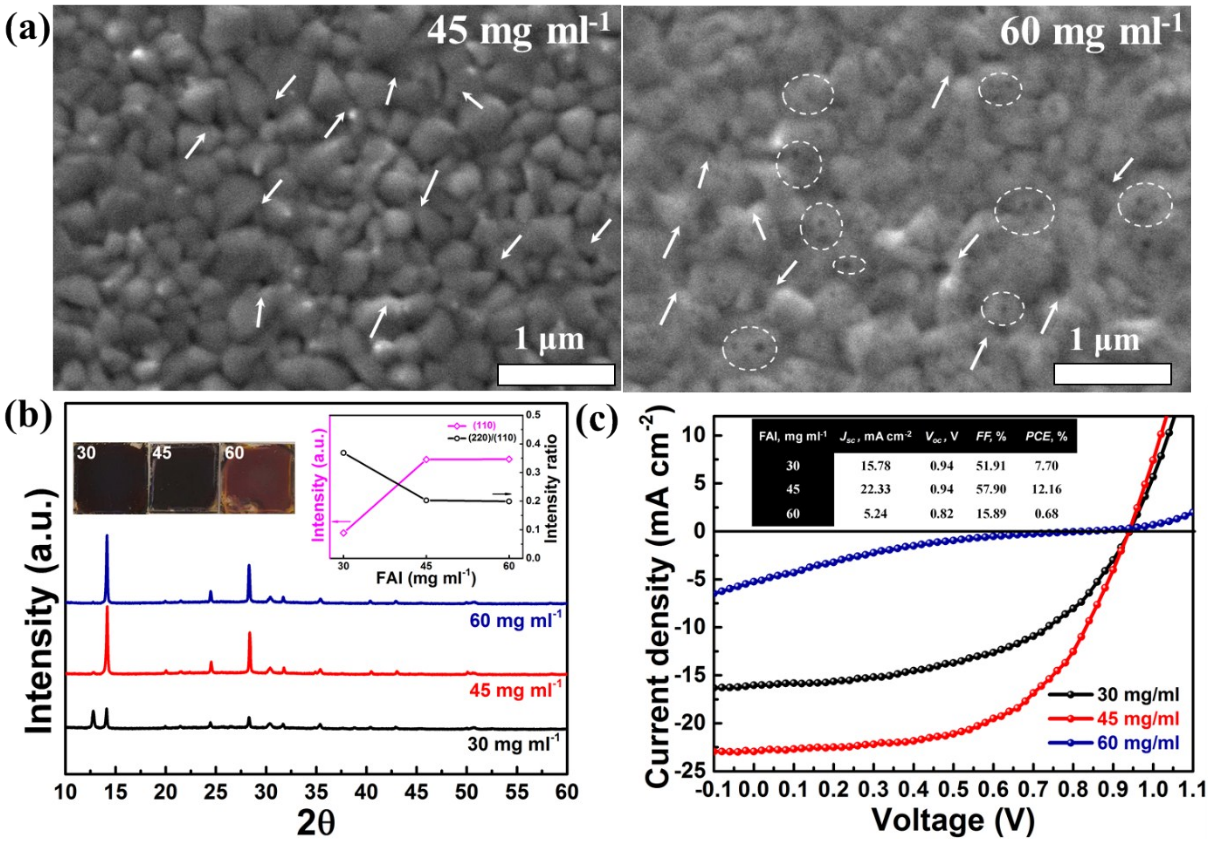

FAI, mg ml^{-1}	J_{sc}, mA cm^{-2}	V_{oc}, V	*FF*, %	*PCE*, %
30	15.78	0.94	51.91	7.70
45	22.33	0.94	57.90	12.16
60	5.24	0.82	15.89	0.68

Figure S5. SEM images (a) and XRD patterns (b) of $Cs_{0.15}FA_{0.85}PbI_3$ prepared by the preheating-only method; (c) *J-V* characteristics of the resulting PSCs; Insets in (b) are the peak intensity of (110) and the intensity ratio of (202)/(110), and their corresponding digital photographs.

When the FAI concertation is increased to 45 mg ml^{-1}, the PbI_2 peak almost disappears, however, several pinholes are observed at the perovskite grain boundaries, as indicated by white arrows in **Figure S5a**. With the perovskite films prepared by 45 mg ml^{-1} FAI, the PSCs achieve a *PCE* of 12.16%. Further increasing the FAI concentration to 60 mg ml^{-1}, albeit no changes observed in XRD patterns, the perovskite film is obviously changed to a wine-colored film, as judged by bare eye (inset in **Figure S5b**). The SEM image in **Figure S5a** shows that in addition to the pinhole at grain boundaries (indicated by white arrows), the film shows many tiny pinholes within the grain (indicated by white dash circles), which leads to an extremely poor *PCE* of 0.68% (**Figure S5c**). Importantly, these observations also demonstrate that with higher concentration of FAI at second step, the perovskite film tends to have more pinholes.

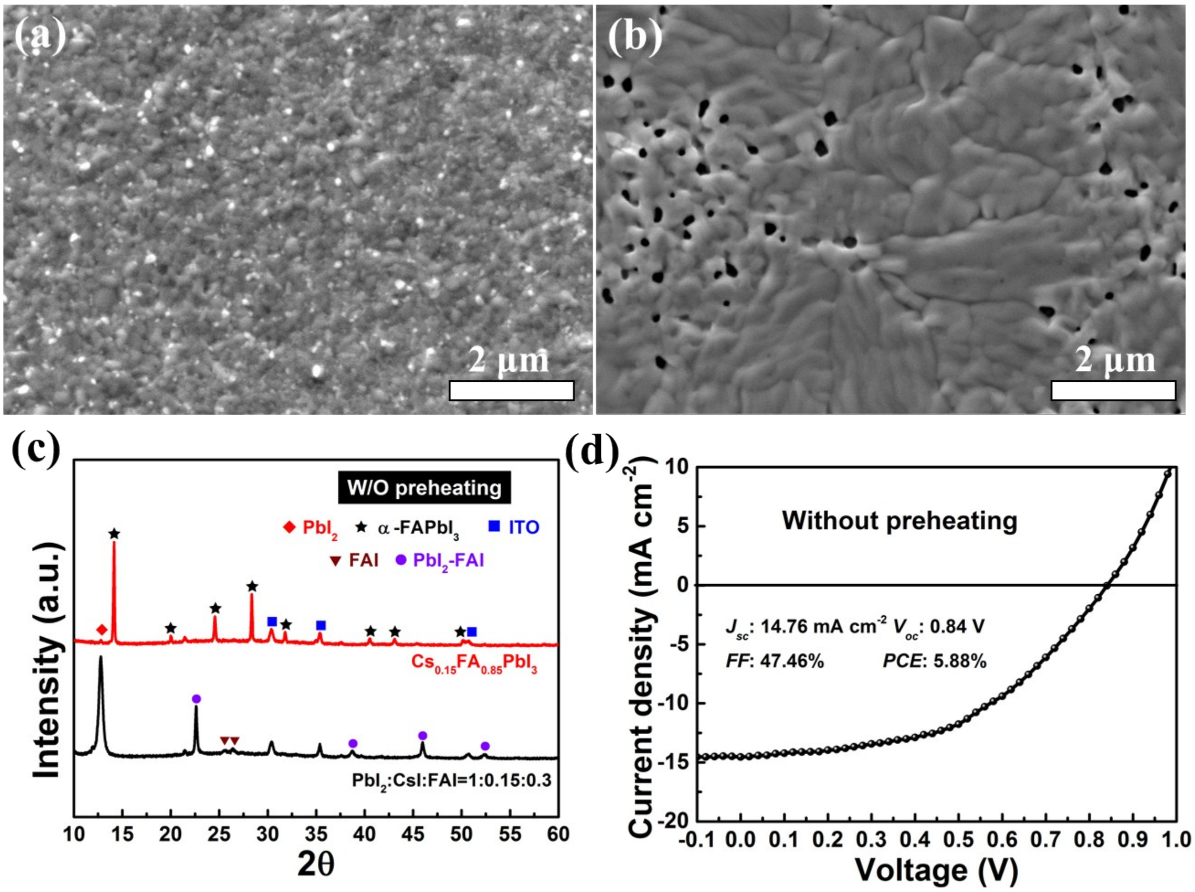

Figure S6. SEM images of the PbI_2-$(CsI)_{0.15}$-$(FAI)_{0.3}$ intermediate complex (a) and $Cs_{0.15}FA_{0.85}PbI_3$ film (b) prepared by the premixing-only method; (c) XRD patterns of the PbI_2-$(CsI)_{0.15}$-$(FAI)_x$ intermediate complex and $Cs_{0.15}FA_{0.85}PbI_3$ prepared by the premixing-only method;. (d) *J-V* characteristics of the $Cs_{0.15}FA_{0.85}PbI_3$ PSC prepared by the premixing-only method.

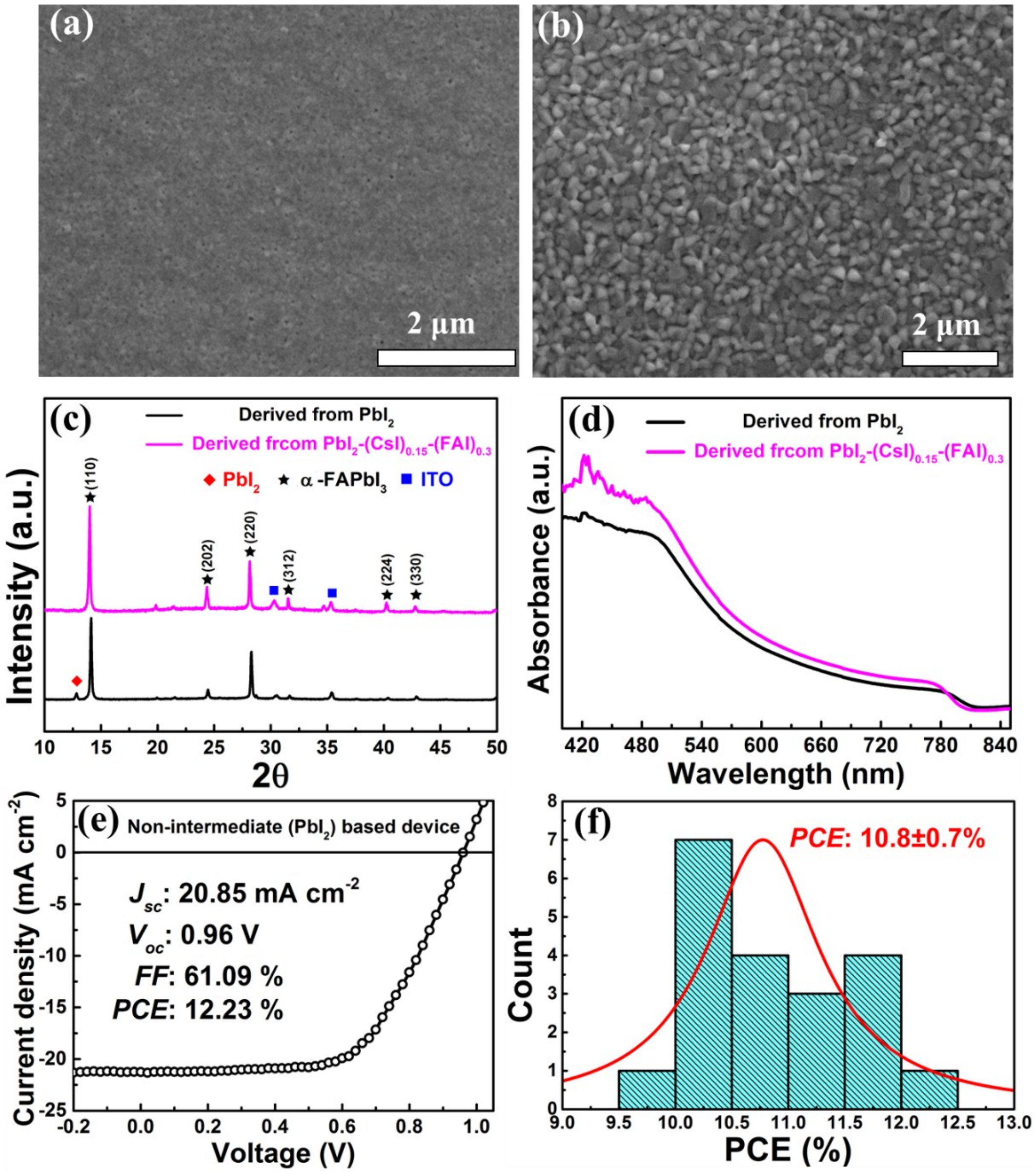

Figure S7. SEM images of PbI_2 (a) and $Cs_{0.15}FA_{0.85}PbI_3$ film (b) prepared by the non-intermediate method; Comparison of XRD patterns (c) and UV-Vis absorbance (d) of $Cs_{0.15}FA_{0.85}PbI_3$ prepared by the non-intermediate and coupled methods; (e) *J-V* characteristics of the champion device and (f) statistics of *PCEs* of 20 devices prepared by the non-intermediate method.

As shown in Figure S7a, without the addition of CsI in the precursor solution, the PbI_2 deposited at the first step shows quite different morphology as compared to that with CsI addition. Instead of the distinctive porous structure consisting of a network of needle-like nanorods (Figure 2a), the PbI_2 exhibits a uniform and smooth film morphology with the presence of some pinholes. After the spin-coating of FAI/CsI (85/15, mol/mol) mixture solution, the non-intermediate derived perovskite mainly consists of small-sized crystals with some pinholes, and exhibits a rough surface morphology (Figure S7b), which is similar to that of perovskite prepared by the preheating-only methods. Moreover, compared to perovskite derived from the coupled method, the non-intermediate derived perovskite shows relatively low crystallinity and absorbance, along with the presence of unreacted PbI_2 (Figure S7 c-d). Due to the poor film quality, the devices based on non-intermediate derived perovskite achieve a champion and average *PCE* of 12.2% and $10.8 \pm 0.7\%$, respectively, which is comparable to that of the device prepared by the preheating-only method but obviously inferior to that that of the device prepared by the coupled method.

References

[1] L. Wang, F. Liu, T. Liu, J. Wang, X. Cai, G. Wang, T. Ma, C. Jiang, ACS Appl. Mater. Interfaces 2016, 8, 30920.

[2] Y. Du, H. Cai, J. Ni, J. Li, H. Yu, X. Sun, Y. Wu, H. Wen, J. Zhang, RSC Adv. 2015, 5, 66981.

[3] P. Bhatt, K. Pandey, P. Yadav, B. Tripathi, C. K. P, M. K. Pandey, M. Kumar, Sol. Energy Mater. Sol. Cells 2015, 140, 320.

[4] S. Ito, S. Tanaka, H. Nishino, Chem. Lett. 2015, 44, 849.

[5] M. Lv, X. Dong, X. Fang, B. Lin, S. Zhang, X. Xu, J. Ding, N. Yuan, RSC Adv. 2015, 5, 93957.

[6] J. Huang, X. Yu, J. Xie, D. Xu, Z. Tang, C. Cui, D. Yang, ACS Appl. Mater. Interfaces 2016, 8, 21505.

[7] L.-L. Gao, C.-X. Li, C.-J. Li, G.-J. Yang, J. Mater. Chem. A 2017, 5, 1548.

[8] B. Jeong, S. M. Cho, S. H. Cho, J. H. Lee, I. Hwang, S. K. Hwang, J. Cho, T.-W. Lee, C. Park, Phys. Status Solid. (RRL) 2016, 10, 381.

[9] L. Xu, H. Liu, W. Qiu, K. Xue, X. Liu, J. Wang, H. Zhang, W. Huang, ACS Sustainable Chem. Eng. 2017, 5, 9718.

[10] L. Binglong, E. Vincent Obiozo, M. Tatsuo, Jpn. J. Appl. Phys. 2015, 54, 100305.

[11] Y. Rong, X. Hou, Y. Hu, A. Mei, L. Liu, P. Wang, H. Han, Nat. Commun. 2017, 8, 14555.

[12] H. Wu, C. Zhang, K. Ding, L. Wang, Y. Gao, J. Yang, Org. Electron. 2017, 45, 302.

[13] H.-S. Ko, J.-W. Lee, N.-G. Park, J. Mater. Chem. A 2015, 3, 8808.

[14] Z. Ren, M. Zhu, X. Li, C. Dong, J. Power Sources 2017, 363, 317.

[15] Z. Liu, T. Shi, Z. Tang, B. Sun, G. Liao, Nanoscale 2016, 8, 7017.

[16] Z. Yunhai, L. Huiru, C. Can, X. Lingbo, W. Peng, W. Hao, Y. Xuegong, X. Jiangsheng, H. Jiabin, T. Zeguo, Y. Deren, Nanotechnology 2017, 28, 205401.

[17] Z. Liang, S. Zhang, X. Xu, N. Wang, J. Wang, X. Wang, Z. Bi, G. Xu, N. Yuan, J. Ding, RSC Adv. 2015, 5, 60562.

[18] G. Wang, D. Liu, J. Xiang, D. Zhou, K. Alameh, B. Ding, Q. Song, RSC Adv. 2016, 6, 43299.

[19] M. Sun, F. Zhang, H. Liu, X. Li, Y. Xiao, S. Wang, J. Mater. Chem. A 2017, 5, 13448.

[20] J. Ciro, R. Betancur, S. Mesa, F. Jaramillo, Sol. Energy Mater. Sol. Cells 2017, 163, 38.

[21] Y. Cheng, X. Xu, Y. Xie, H.-W. Li, J. Qing, C. Ma, C.-S. Lee, F. So, S.-W. Tsang, Solar RRL 2017, 1, 1700097.

[22] N. Islavath, S. Saroja, K. S. Reddy, P. C. Harikesh, G. Veerappan, S. V. Joshi, E. Ramasamy, J. Energy Chem. 2017, 26, 584.

[23] J. Troughton, K. Hooper, T. M. Watson, Nano Energy 2017, 39, 60.

[24] S. Pathak, A. Sepe, A. Sadhanala, F. Deschler, A. Haghighirad, N. Sakai, K. C. Goedel, S. D. Stranks, N. Noel, M. Price, S. Hüttner, N. A. Hawkins, R. H. Friend, U. Steiner, H. J. Snaith, ACS Nano 2015, 9, 2311.

[25] M. Seetharaman S, P. Nagarjuna, P. N. Kumar, S. P. Singh, M. Deepa, M. A. G. Namboothiry, PCCP 2014, 16, 24691.

[26] L. Zhang, X. Zhang, Y. Yu, X. Xu, J. Tang, X. He, J. Wu, Z. Lan, Sol. Energy 2017, 155, 942.

[27] Q. Tai, P. You, H. Sang, Z. Liu, C. Hu, H. L. W. Chan, F. Yan, Nat. Commun. 2016, 7, 11105.

[28] J. Liang, P. Zhao, C. Wang, Y. Wang, Y. Hu, G. Zhu, L. Ma, J. Liu, Z. Jin, J. Am. Chem. Soc. 2017, 139, 14009.

[29] J. Liang, C. Wang, Y. Wang, Z. Xu, Z. Lu, Y. Ma, H. Zhu, Y. Hu, C. Xiao, X. Yi, G. Zhu, H. Lv, L. Ma, T. Chen, Z. Tie, Z. Jin, J. Liu, J. Am. Chem. Soc. 2016, 138, 15829.